Quantum theory of the far-off-resonance continuous-wave Raman laser: Heisenberg-Langevin approach

P. A. Roos,* S. K. Murphy, L. S. Meng, and J. L. Carlsten†
Department of Physics, Montana State University, Bozeman, Montana 59717, USA

T. C. Ralph and A. G. White
Department of Physics, University of Queensland, St. Lucia, Queensland 4072, Australia

J. K. Brasseur
Directed Energy Solutions, 532 Fox Run Circle, Colorado Springs, Colorado 80921, USA

We present the quantum theory of the far-off-resonance continuous-wave Raman laser using the Heisenberg-Langevin approach. We show that the simplified quantum Langevin equations for this system are mathematically identical to those of the nondegenerate optical parametric oscillator in the time domain with the following associations: pump ↔ pump, Stokes ↔ signal, and Raman coherence ↔ idler. We derive analytical results for both the steady-state behavior and the time-dependent noise spectra, using standard linearization procedures. In the semiclassical limit, these results match with previous purely semiclassical treatments, which yield excellent agreement with experimental observations. The analytical time-dependent results predict perfect photon statistics conversion from the pump to the Stokes and nonclassical behavior under certain operational conditions.

I. INTRODUCTION AND MOTIVATION

There has been a significant amount of theoretical work addressing the quantum mechanical nature of pulsed Raman laser systems ([1], and references therein), but little attention was devoted to the continuous-wave (cw) regime until the late 1980s and the 1990s. At that time, three-level atoms interacting with quantized field modes were analyzed in the process of identifying and characterizing nonclassical sources of light. For such atoms in the Λ-configuration, many competing processes can contribute to the overall dynamics of the system. These processes include optical bistability [2], traditional population-based lasing [3], lasing without inversion [4–6], and electromagnetically induced transparency [7] in addition to two-photon Raman lasing [8–11]. More general treatments of three level systems have also been performed, which can accommodate many of these processes [12–15].

The present treatment is motivated by the experimental realization of far-off-resonance cw Raman lasers in diatomic hydrogen gas using high-finesse cavity enhancement of both the pump and the Stokes fields [16]. The hydrogen molecules can be modeled as three-level Λ systems. The primary features that make this system unique are (1) the optical frequencies involved are extraordinarily far off resonance from any single-photon atomic transitions (hence the need for high-finesse cavity enhancement) and (2) the nonradiative decay of the final Raman level is very fast compared to the Raman excitation rate of this level. The fundamental difference between this cavity-enhanced cw Raman work and the past-pulsed Raman work lies in the fact that pulsed Raman systems typically do not include a laser oscillator. Instead, the pulsed systems are most often pumped longitudinally through long cells filled with the Raman gas, sometimes with multiple (nonoverlapping) passes. The emission from these pulsed Raman systems might therefore be more accurately classified as amplified spontaneous emission, rather than laser emission. For this reason, the theoretical methods and limits that we employ to treat our well-established laser mode are often very different from those used to treat pulsed Raman systems. Many of the fine details that are omitted from the present work for the sake of brevity can be found in Chapter 3 of Ref. [17].

In a closely related work, Rebic and co-workers [11] examine a similar system, but focus on the case where no decay path from the final Raman state to the ground state is present to close the pump cycle. In their analysis, the final Raman state population returns to the ground state via coherent interactions with the cavity field modes (anti-Stokes generation). Decay of the final Raman state population is critical to the results presented in this work. In another related work, Poizat, Collett, and Walls [18] examine two field modes interacting with a collection of three-level atoms in ladder or cascade configurations. Olsen, Gheri, and Walls [19] note that this system can exhibit similar behavior to the corresponding Λ-configuration in certain circumstances.

As an alternative to the Heisenberg-Langevin approach provided in the present work, one can also restrict the general treatment of Eschmann and Balbagh [15] or others [12–14] to the appropriate limits and address the system in the Schrödinger picture. We prefer the Heisenberg picture for the present work because it lends itself more directly to the study of noise spectra and perhaps to the development of physical understanding.

After this introduction, we use Sec. II to assemble the

---

*Present address: JILA, National Institute of Standards and Technology, and University of Colorado, Boulder, CO 80309-0440.
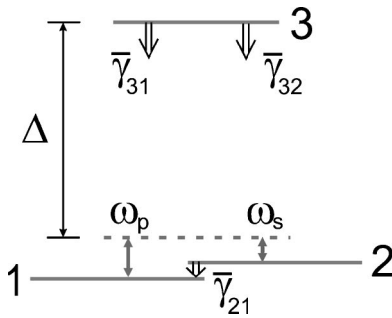†Electronic address: carlsten@physics.montana.edu

FIG. 1. To-scale energy level diagram for the diatomic hydrogen molecule showing the pertinent levels and the far-off-resonance fields.

appropriate components of the total Hamiltonian. We then generate the quantum Langevin equations for the system operators in Sec. III following the work of Gardiner and Collett [20]. In Sec. IV, we exploit the large single-photon detuning to simplify the equations of motion significantly. In Sec. V, we draw a direct connection between the far-off-resonance cw Raman system and the cw nondegenerate optical parametric oscillator (NDOPO). In Sec. VI, we linearize the simplified quantum Langevin equations and solve for the noise spectra of the emitted pump and the Stokes light analytically. In Sec. VII, we compare our analytical results to numerical results of a previous semiclassical treatment and we take several useful limits of the equations in order to solidify the understanding of the underlying physics. We review our findings and provide some concluding thoughts in the final section.

II. HAMILTONIAN

In the interest of retaining as much clarity as possible, we make several initial simplifications. We focus on the temporal aspects of the system in this work. The effects of neglecting the spatial aspects are superficial and will be discussed in the text. We neglect thermal population of the upper states because the states differ substantially in energy from the ground state. The generation of all anti-Stokes orders and Stokes orders higher than the first are neglected in the present treatment because these fields are not enhanced within the cavity. The effect of cavity enhancing the first anti-Stokes order yields interesting results and is treated elsewhere [21]. We neglect the complicating effects of heat generation, which have been observed experimentally for the systems that generate large Stokes powers [22,23].

We approximate the hydrogen molecules as three-level Λ systems and we allow them to interact with two quantized high-finesse cavity modes, as shown in Fig. 1. For the pure vibrational cw Raman lasers that have been experimentally demonstrated in diatomic hydrogen, the most probable transition at room temperature is $Q_{01}(1)$ with a shift of 4155 cm^{-1}. For this case, level 1 is the ground state ($v = 0$, $J = 1$), level 2 is the first excited vibrational state ($v = 1$, $J = 1$), and level 3 is the first excited electronic state, which is spaced $91\,689$ cm^{-1} from the ground state. Other Raman transitions [$Q_{01}(0)$, for instance] are ignored be-

cause the thermal distributions of population for the levels involved are much smaller and their Raman shifts differ significantly (much more than the Raman linewidth) from that of $Q_{01}(1)$. Although we focus on the vibrational transition, the model presented in this work is also valid for the purely rotational cw Raman lasers that have been realized [24]. Figure 1 shows the energy-level spacings and the optical frequencies to-scale in order to emphasize the large single-photon detuning (Δ in the figure) present. This detuning ($\sim 10^{16}$ Hz) is by far the largest rate in the system (including Rabi frequencies) for the optical powers considered. After Sec. III we will assume that the two-photon 1–2 transition is resonant, which is easily achieved experimentally. Single-photon 1–2 transitions and all other single-photon transitions within the ground-state manifold are forbidden by selection rules for this homonuclear molecule. Decays of all the populations and coherences are allowed. Detunings are represented by Δ's, population decay rates by $\bar{\gamma}$'s (denoted by the bar) and collisional dephasing rates by $\tilde{\gamma}$'s (with tildes, not shown in the figure). In this way, for instance, $\bar{\gamma}_{21}$ represents the population decay rate from level 2 to level 1. Similarly, $\tilde{\gamma}_{22}$ will contribute to decay of the coherences that involve level 2.

As Fig. 1 suggests, we invoke the rotating wave approximation (RWA) here to simplify the calculation despite the fact that it is not valid for the large single-photon detuning present. We perform a similar invalid simplification by only considering pump photon interactions with the 1–3 atomic transition and the Stokes photon interactions with the 2–3 atomic transition. In reality, additional upper states and other similar atom-photon interactions exist in this system. However, Ref. [17] shows that none of these simplifications affects the qualitative behavior of the system; they only cause quantitative modifications to the Raman gain. In practice, this gain is determined from an empirically based parameter. Furthermore, the noise spectra results that we derive do not depend on the Raman gain and are therefore unaffected by these simplifications.

The hydrogen molecules occupy the space between two mirrors of a linear high-finesse cavity. The results given in this work can be easily adapted to other cavity geometries. The incident pump light is actively frequency stabilized to a resonance of the cavity. The front mirror (denoted "0" throughout this work) serves as the input coupler for the pump light, while the back mirror (denoted "1") is eventually treated as the output coupler for the Stokes. The total Hamiltonian describing the atoms, the fields, the baths (for decay and noise purposes), and their mutual interactions is

$$H = H_1 + H_2 + H_3 + H_4 + H_5 + H_{\text{baths}}, \tag{1}$$

where the components of H are given in the following paragraphs.

H_1 represents the free energy of the atoms and fields in the absence of any interactions and is given by

$$H_1 = \sum_{i=1}^{3} \hbar \omega_i S_{ii} + \sum_{q=p,s} \hbar \omega_q^c a_q^\dagger a_q, \tag{2}$$

where $\hbar\omega_i$ and S_{ii} are the energy and collective population operator for the ith atomic state, respectively. Throughout this work, the subscript p refers to the pump and s refers to the Stokes, while q is a general index referring to either. In this way, the operators a_q and $a_q^\dagger$ refer to the annihilation and creation of the pump ($q=p$) and the Stokes ($q=s$) photons, respectively, while ω_p^c and ω_s^c are the frequencies of the empty cavity modes nearest to the pump and the Stokes optical frequencies, respectively.

H_2 represents the reversible interaction energy associated with atom-field couplings in the electric dipole and rotating wave approximations and is given by

$$H_2 = i\hbar(g_{p,13}a_p^\dagger S_{13} - \text{H.c.}) + i\hbar(g_{s,23}a_s^\dagger S_{23} - \text{H.c.}), \quad (3)$$

where the collective coherence operator between levels i and j is given by S_{ij} and $g_{q,ij}$ represents the atom-field coupling constant for the field mode q driving the $i-j$ atomic transition. We emphasize again here that only the pump interactions with the $1-3$ transition and the Stokes interactions with the $2-3$ transition are considered. Additional terms (that do not affect the results of this work) arise in Eq. (3) when the RWA is not invoked and when other atom-photon interactions are included [17].

H_3 represents the coupling between the two active cavity modes and the external field baths for decay and noise purposes and is given by

$$H_3 = i\hbar \sum_{q=p,s} \int_{-\infty}^{\infty} d\omega \left\{ \sqrt{\frac{\kappa_{q,0}}{\pi}}[b_{q,0}^\dagger(\omega)a_q - a_q^\dagger b_{q,0}(\omega)] \right.$$

$$+ \sqrt{\frac{\kappa_{q,1}}{\pi}}[b_{q,1}^\dagger(\omega)a_q - a_q^\dagger b_{q,1}(\omega)]$$

$$\left. + \sqrt{\frac{\kappa_{q,L}}{\pi}}[b_{q,L}^\dagger(\omega)a_q - a_q^\dagger b_{q,L}(\omega)] \right\}, \quad (4)$$

where the external field bath operators $b_{q,0}$ and $b_{q,0}^\dagger$ are coupled to the qth internal cavity mode through the coupling constant $\kappa_{q,0}$. Physically, this constant represents the cavity amplitude decay rate due to transmission through the front (input coupler) mirror (signified by the subscript 0). Similarly, subscripts 1 and L signify that the coupling constants $\kappa_{q,1}$ and $\kappa_{q,L}$ represent the cavity decays due to the back mirror transmission and absorption losses within the cavity, respectively. We couple the external field bath operators $b_{q,1}$ and $b_{q,1}^\dagger$ as well as $b_{q,L}$ and $b_{q,L}^\dagger$ to the qth internal mode to model these cavity losses. The cavity decay rates are related to the mirror transmissivities (T's) and absorptions (A's) through

$$\kappa_{q,0} \approx T_{q,0}/2\tau_{\text{rt}}, \quad \kappa_{q,1} \approx T_{q,1}/2\tau_{\text{rt}}, \quad \kappa_{q,L} \approx A_q/2\tau_{\text{rt}}, \quad (5)$$

where $\tau_{\text{rt}} = 2L/c$ is the round-trip time within the cavity and the approximate equalities hold when the cavity mirror reflectivities approach unity. These decay constants constitute all the cavity losses, so we may write the overall cavity amplitude decay rate as

$$\kappa_q = \kappa_{q,0} + \kappa_{q,1} + \kappa_{q,L}. \quad (6)$$

In Eq. (4) we assume that the cavity decay rates, and therefore the mirror transmissivities and absorptions, are constant over large frequency bandwidths compared to the cavity resonance widths (the κ's do not depend on ω). This is the first Markoff approximation and is easily achieved in practice for this system. We also employ this approximation for H_4 and H_5.

H_4 represents the coupling between atomic coherences and atomic bath operators to generate damping and noise in the atoms and is given by

$$H_4 = i\hbar \int_{-\infty}^{\infty} d\omega \left\{ \sqrt{\frac{\bar{\gamma}_{21}}{2\pi}}[B_{12}^\dagger(\omega)S_{12} - S_{12}^\dagger B_{12}(\omega)] \right.$$

$$+ \sqrt{\frac{\bar{\gamma}_{31}}{2\pi}}[B_{13}^\dagger(\omega)S_{13} - S_{13}^\dagger B_{13}(\omega)]$$

$$\left. + \sqrt{\frac{\bar{\gamma}_{32}}{2\pi}}[B_{23}^\dagger(\omega)S_{23} - S_{23}^\dagger B_{23}(\omega)] \right\}, \quad (7)$$

where the decay rates of the state populations, given by the $\bar{\gamma}_{ji}$'s, can be interpreted as coupling constants between the atomic system operators and the atomic bath operators, which are given by B_{ij} and $B_{ij}^\dagger$. The decays of population downward from level 3 and downward from level 2 are due to spontaneous emission, and inelastic molecular collisions, respectively.

Similarly, H_5 represents the coupling between atomic populations and atomic bath operators to generate decay and noise of the atomic coherences through dephasing and is given by

$$H_5 = i\hbar \sum_{i=1}^{3} \int_{-\infty}^{\infty} d\omega \sqrt{\frac{\tilde{\gamma}_{ii}}{2\pi}}[B_{ii}^\dagger(\omega)S_{ii} - S_{ii}B_{ii}(\omega)], \quad (8)$$

where the $\tilde{\gamma}_{ii}$'s are the dephasing rates associated with each level due to elastic molecular collisions, while $B_{ii}^\dagger$ and B_{ii} are the corresponding atomic bath operators. We model this interaction after Gardiner and Zoller [25] and Eschmann and Ballagh [15].

H_{baths} represents the free energy of the external bath or reservoir modes and is given by

$$H_{\text{baths}} = \sum_{q=p,s} \int_{-\infty}^{\infty} d\omega \hbar \omega [b_{q,0}^\dagger(\omega)b_{q,0}(\omega) + b_{q,1}^\dagger(\omega)b_{q,1}(\omega)$$

$$+ b_{q,L}^\dagger(\omega)b_{q,L}(\omega)] + \int_{-\infty}^{\infty} d\omega \hbar \omega [B_{12}^\dagger(\omega)B_{12}(\omega)$$

$$+ B_{13}^\dagger(\omega)B_{13}(\omega) + B_{23}^\dagger(\omega)B_{23}(\omega)]$$

$$+ \sum_{i=1}^{3} \int_{-\infty}^{\infty} d\omega \hbar \omega B_{ii}^\dagger(\omega)B_{ii}(\omega). \quad (9)$$

Under the independent atom approximation, the system operators (i.e., those other than the reservoir operators) obey

the standard equal-time commutation relations and multiplication rules, $[a_q, a_{q'}^\dagger] = \delta_{qq'}$, $S_{ij}S_{kl} = S_{il}\delta_{jk}$, and $[S_{ij}, S_{kl}] = S_{il}\delta_{jk} - S_{jk}^\dagger\delta_{il}$, where δ denotes the Kronecker delta and we note that $S_{jk}^\dagger = S_{kj}$. The reservoir operators obey the standard boson commutation relations [20].

III. QUANTUM LANGEVIN EQUATIONS

Following the work of Gardiner and Collett [20], as well as the later work of Poizat, Collett, and Walls [18] and of Ralph, Harb, and Bachor [3], we now use the Heisenberg equation of motion with the above Hamiltonian and commutation relations to generate the quantum Langevin equations for the system operators. In rotating coordinate frames, we find that the Langevin equations for the slowly varying pump and Stokes field operators are given by

$$\dot{a}_p = -(\kappa_p + i\Delta_p)a_p + g_{p,13}S_{13} + \sqrt{2\kappa_{p,0}}a_{p,0}^{in} + \sqrt{2\kappa_{p,1}}a_{p,1}^{in} + \sqrt{2\kappa_{p,L}}a_{p,L}^{in}, \tag{10}$$

$$\dot{a}_s = -(\kappa_s + i\Delta_s)a_s + g_{s,23}S_{23} + \sqrt{2\kappa_{s,0}}a_{s,0}^{in} + \sqrt{2\kappa_{s,1}}a_{s,1}^{in} + \sqrt{2\kappa_{s,L}}a_{s,L}^{in}, \tag{11}$$

where Eq. (6) has been used and $\Delta_q \equiv \omega_q^c - \omega_q$ represents the detuning of the driving optical frequency (ω_q) from the qth cold cavity resonance (ω_q^c). The superscript *in* denotes an input operator ([26], p. 123).

We obtain the Langevin equations for the atomic coherences in a similar fashion with the results

$$\dot{S}_{12} = -(\gamma_{21} + i\Delta_{12})S_{12} + g_{p,13}^* a_p S_{23}^\dagger + g_{s,23}a_s^\dagger S_{13} + F_{12}, \tag{12}$$

$$\dot{S}_{13} = -(\gamma_{31} + i\Delta)S_{13} - g_{p,13}^* a_p(S_{11} - S_{33}) - g_{s,23}^* a_s S_{12} + F_{13}, \tag{13}$$

$$\dot{S}_{23} = -(\gamma_{32} + i\Delta)S_{23} - g_{s,23}^* a_s(S_{22} - S_{33}) - g_{p,13}^* a_p S_{12}^\dagger + F_{23}, \tag{14}$$

where $\Delta_{12} \equiv (\omega_2 - \omega_1) - (\omega_p - \omega_s)$ is the two-photon Raman detuning, and $\Delta \equiv (\omega_3 - \omega_1) - \omega_p \approx (\omega_3 - \omega_2) - \omega_s$ is the single-photon detuning (see Fig. 1). We have defined the overall coherence decay constants as $\gamma_{21} \equiv (\bar{\gamma}_{21} + \tilde{\gamma}_{11} + \tilde{\gamma}_{22})/2$, $\gamma_{31} \equiv (\bar{\gamma}_{31} + \bar{\gamma}_{32} + \tilde{\gamma}_{11} + \tilde{\gamma}_{33})/2$, and $\gamma_{32} \equiv (\bar{\gamma}_{32} + \bar{\gamma}_{31} + \bar{\gamma}_{21} + \tilde{\gamma}_{33} + \tilde{\gamma}_{22})/2$, and the noise terms are

$$F_{12} \equiv +\sqrt{\bar{\gamma}_{21}}(S_{11} - S_{22})B_{12}^{in} - \sqrt{\bar{\gamma}_{31}}S_{23}^\dagger B_{13}^{in} - \sqrt{\bar{\gamma}_{32}}B_{23}^\dagger S_{13} - \sqrt{\tilde{\gamma}_{11}}(S_{12}B_{11}^{in} - B_{11}^{in\dagger}S_{12}) + \sqrt{\tilde{\gamma}_{22}}(S_{12}B_{22}^{in} - B_{22}^{in\dagger}S_{12}), \tag{15}$$

$$F_{13} \equiv \sqrt{\bar{\gamma}_{31}}(S_{11} - S_{33})B_{13}^{in} + \sqrt{\bar{\gamma}_{32}}S_{12}B_{23}^{in} - \sqrt{\bar{\gamma}_{21}}S_{23}B_{12}^{in} - \sqrt{\tilde{\gamma}_{11}}(S_{13}B_{11}^{in} - B_{11}^{in\dagger}S_{13}) + \sqrt{\tilde{\gamma}_{33}}(S_{13}B_{33}^{in} - B_{33}^{in\dagger}S_{13}), \tag{16}$$

Parameter	Symbol	Value (Hz)
Effective atom-field coupling	$g_{q,ij}/2\pi$	$\sim 10^4 - 10^5$
Level 2 population decay	$\bar{\gamma}_{21}/2\pi$	$\sim 10^4 - 10^5$
Cavity amplitude decay	$\kappa_q/2\pi$	$\sim 10^5 - 10^6$
Level 2 coherence decay	$\gamma_{21}/2\pi$	$\sim 10^8 - 10^9$
Level 3 coherence decay	$\gamma_{31}/2\pi$, $\gamma_{32}/2\pi$	$\sim 10^9 - 10^{10}$
Single-photon Rabi frequencies	$\Omega_{q,ij}/2\pi$	$\lesssim 10^{10}$
Single-photon detuning	$\Delta/2\pi$	$\sim 10^{15} - 10^{16}$

$$F_{23} \equiv \sqrt{\bar{\gamma}_{32}}(S_{22} - S_{33})B_{23}^{in} + \sqrt{\bar{\gamma}_{31}}S_{12}^\dagger B_{13}^{in} + \sqrt{\bar{\gamma}_{21}}B_{12}^{in\dagger}S_{13} - \sqrt{\tilde{\gamma}_{22}}(S_{23}B_{22}^{in} - B_{22}^{in\dagger}S_{23}) + \sqrt{\tilde{\gamma}_{33}}(S_{23}B_{33}^{in} - B_{33}^{in\dagger}S_{23}). \tag{17}$$

We also find that the population equations are given by

$$\dot{S}_{11} = \bar{\gamma}_{21}S_{22} + \bar{\gamma}_{31}S_{33} + (g_{p,13}a_p^\dagger S_{13} + \text{H.c.}) + F_{11}, \tag{18}$$

$$\dot{S}_{22} = \bar{\gamma}_{32}S_{33} - \bar{\gamma}_{21}S_{22} + (g_{s,23}a_s^\dagger S_{23} + \text{H.c.}) + F_{22}, \tag{19}$$

$$\dot{S}_{33} = -\dot{S}_{11} - \dot{S}_{22}, \tag{20}$$

where we used atom conservation ($S_{11} + S_{22} + S_{33} = N$, where N is the number of molecules) to obtain Eq. (19), and the noise terms are given by

$$F_{11} \equiv -\sqrt{\bar{\gamma}_{21}}(S_{12}^\dagger B_{12}^{in} + B_{12}^{in\dagger}S_{12}) - \sqrt{\bar{\gamma}_{31}}(S_{13}^\dagger B_{13}^{in} + B_{13}^{in\dagger}S_{13}), \tag{21}$$

$$F_{22} \equiv -\sqrt{\bar{\gamma}_{32}}(S_{23}^\dagger B_{23}^{in} + B_{23}^{in\dagger}S_{23}) + \sqrt{\bar{\gamma}_{21}}(S_{12}^\dagger B_{12}^{in} + B_{12}^{in\dagger}S_{12}). \tag{22}$$

The following section is devoted to simplifying these quantum Langevin equations.

IV. SIMPLIFIED QUANTUM LANGEVIN EQUATIONS

We now exploit the large single-photon detuning and the moderate Rabi frequencies to significantly simplify the quantum Langevin equations. For reference purposes, approximate values for the pertinent rates in this system are provided in Table I. The extreme single-photon detuning allows us to make the following simplifications.

(1) Adiabatically eliminate the level 3 coherences. As shown by Raymer, Mostowski, and Carlsten [27], the 1–3 and 2–3 coherences can be adiabatically eliminated when the single-photon detunings are much larger than the other rates in the system. We can therefore solve for the "coarse-grained" steady-state coherences from Eqs. (13) and (14) and insert these into the remaining six equations.

(2) Disregard the single-photon absorption and mode pulling. Terms arise in the two field operator equations that represent linear absorption (real parts) and dispersion (imaginary parts). For near-resonance systems (when

$\Delta \lesssim \gamma_{31}, \gamma_{32}$), the real portions can supply the population inversion necessary for traditional laser gain. In the present system, the real parts of these terms effectively broaden, while the imaginary parts pull, the frequency of the cavity resonances due to single-photon interactions with the medium. In the limit $\Delta^2 \kappa_q \gg \gamma_{ji} |g_{q,ij}|^2$, the absorption terms can be disregarded. The mode pulling is small and in practice is nullified by active electronic stabilization of the cavity length to the pump laser frequency (i.e., we adjust the physical cavity length to compensate for the refractive index change). We also assume that the Stokes field will build on the *active* cavity resonance line center.

(3) Ignore power broadening and Stark shifts. Terms arise in the $1-2$ coherence equation that are quadratic in the field operators (linear in optical power), and linear in the coherence. In direct analogy with simplification (2), these terms cause power broadening (real parts) and Stark shifts (imaginary parts) of the two-photon ($1-2$) atomic transition. In the limit $\Delta^2 \gamma_{21} \gg \gamma_{ij} |\Omega_{q,ij}|^2$, where $\Omega_{q,ij} \equiv g_{q,ij} a_q$ is the Rabi frequency for the optical field q driving the ij single-photon atomic transition, the power broadening can be ignored. The Stark shift is predicted to be very mild (<1 MHz) compared to the two-photon resonance width, γ_{21}, for the optical powers considered, and can be compensated easily in practice by tuning the pump laser (with the cavity following). For electromagnetically induced transparency ([7], and references therein) the Stark shift is much larger and plays a critical role.

(4) Neglect spontaneous emission. In the limit of large single-photon detuning relative to the level 3 decay rate, we can make the approximation $(\gamma_{31} + i\Delta)^{-1} \approx (i\Delta)^{-1}$ and likewise for similar terms. Moreover, as one might expect from the fluctuation-dissipation theorem [28], because the upper level decay can be neglected, the associated noise terms entering from the $1-3$ and $2-3$ coherences are severely diminished by the single-photon detuning as well. In the above limits, we therefore ignore F_{13} and F_{23} when compared to the field and $1-2$ coherence noise terms.

(5) Ignore upper state population. One can show that the fractional population of level 3 is on the order of $\sim |\Omega_{p,13}/\Delta|^2$, which is negligible for the large single-photon detuning and moderate Rabi frequencies considered. Furthermore, in the same limits, the level 2 population is on the order of $\sim \Gamma_{12}/\bar{\gamma}_{21}$, where the level 2 Raman excitation rate is

$$\Gamma_{12} \equiv \left(\frac{2\gamma_{21}}{\gamma_{21}^2 + \Delta_{12}^2} \right) \left| \frac{\Omega_{p,13} \Omega_{s,23}}{\Delta} \right|^2, \quad (23)$$

which is typically at least four orders of magnitude smaller than the population decay rate from level 2 ($\bar{\gamma}_{21}$). In other words, level 2 is populated at a much slower rate than it is depopulated. This ensures that no coherent back conversion of the generated Stokes light (through the anti-Stokes process) will occur for this system. This also means we can safely assume that all the population remains in the ground state at all times.

With these simplifications, the pertinent operator equations for this Raman system become

$$\dot{a}_p = -\kappa_p a_p + i g a_s S_{12} + \sqrt{2\kappa_{p,0}} a_{p,0}^{\text{in}} + \sqrt{2\kappa_{p,1}} a_{p,1}^{\text{in}} + \sqrt{2\kappa_{p,L}} a_{p,L}^{\text{in}}, \quad (24)$$

$$\dot{a}_s = -\kappa_s a_s + i g^* a_p S_{12}^{\dagger} + \sqrt{2\kappa_{s,0}} a_{s,0}^{\text{in}} + \sqrt{2\kappa_{s,1}} a_{s,1}^{\text{in}} + \sqrt{2\kappa_{s,L}} a_{s,L}^{\text{in}}, \quad (25)$$

$$\dot{S}_{12} = -\gamma_{21} S_{12} + i g^* a_p a_s^{\dagger} + \sqrt{2\gamma_{21}} S_{12}^{\text{in}}, \quad (26)$$

where

$$g \equiv \frac{g_{p,13} g_{s,23}^*}{\Delta} \sqrt{N}, \quad (27)$$

and N is the number of molecules. In obtaining Eqs. (24)–(26), we have renormalized the $1-2$ coherence operator ($S_{12}^{old} \rightarrow S_{12}^{new} \sqrt{N}$) and we have defined the input coherence operator

$$S_{12}^{\text{in}} \equiv \frac{1}{\sqrt{2\gamma_{21} N}} F_{12}, \quad (28)$$

where the noise term F_{12} is given by Eq. (15). We have also assumed that the two-photon Raman detuning and the cavity detunings are zero, which is easily achieved in practice. Note that Eqs. (24)–(26) are decoupled from the populations.

To more fully characterize these simplified Raman laser equations, we note that the nonvanishing second-order correlation functions of the input field operators are

$$\langle a_{p,1}^{\text{in}}(t) a_{p,1}^{\text{in}\dagger}(t') \rangle = \langle a_{p,L}^{\text{in}}(t) a_{p,L}^{\text{in}\dagger}(t') \rangle = \delta(t-t'), \quad (29)$$

$$\langle a_{s,0}^{\text{in}}(t) a_{s,0}^{\text{in}\dagger}(t') \rangle = \langle a_{s,1}^{\text{in}}(t) a_{s,1}^{\text{in}\dagger}(t') \rangle = \delta(t-t'), \quad (30)$$

$$\langle a_{s,L}^{\text{in}}(t) a_{s,L}^{\text{in}\dagger}(t') \rangle = \delta(t-t'), \quad (31)$$

where we have used the commutation relations $[a_q^{\text{in}}(t), a_q^{\text{in}\dagger}(t')] = \delta(t-t')$, and we have assumed that the input fluctuations are ordinary vacuum, so that $\langle a_q^{\text{in}\dagger} | \rightarrow \langle 0 |$ and $|a_q^{\text{in}} \rangle \rightarrow |0\rangle$.

To calculate the second-order correlation functions for the coherence input operator, we convert to the Ito calculus so that the system operators commute with the input operators. This conversion is not essential and does not alter Eqs. (24)–(26) or the behavior of the system, but it does simplify the mathematical treatment. Using the definitions given by Eqs. (15) and (28), and the fact that the input operators commute with the system operators for the Ito calculus, we calculate

$$\langle S_{12}^{\text{in}}(t) S_{12}^{\text{in}}(t') \rangle = \langle S_{12}^{\text{in}\dagger}(t) S_{12}^{\text{in}\dagger}(t') \rangle = 0, \quad (32)$$

$$\langle S_{12}^{\text{in}\dagger}(t) S_{12}^{\text{in}}(t') \rangle = \frac{\bar{\gamma}_{32}}{N 2\gamma_{21}} \langle S_{33}(t) \rangle \delta(t-t') \approx 0, \quad (33)$$

$$\langle S_{12}^{\text{in}}(t) S_{12}^{\text{in}\dagger}(t') \rangle = \frac{1}{N2\gamma_{21}} [\bar{\gamma}_{21} \langle S_{11}(t) + S_{33}(t) \rangle + \bar{\gamma}_{31} \langle S_{33}(t) \rangle$$

$$+ \tilde{\gamma}_{11} \langle S_{11}(t) \rangle + \tilde{\gamma}_{22} \langle S_{11}(t) \rangle] \delta(t-t')$$

$$\approx \frac{1}{2\gamma_{21}} (\bar{\gamma}_{21} + \tilde{\gamma}_{11} + \tilde{\gamma}_{22}) \delta(t-t') = \delta(t-t'),$$
$$\tag{34}$$

where we have used the fact that all the population remains in the ground state. Interestingly, the dearth of upper state population means that the 1–2 input coherence operator is δ correlated when the input fluctuations are vacuum, just like the field input operators.

V. CONNECTION TO THE NDOPO

With the input operator correlation functions established, we can now draw a direct connection between the quantum cw Raman laser equations defined by Eqs. (24)–(26) and those of the NDOPO [29] with the following associations: pump↔pump, Stokes↔signal, 1–2 coherence↔idler. The connection between the stimulated Raman and optical parametric processes was actually established shortly after the discovery of both from conceptual and mathematical standpoints by other researchers [30]. At that time, both of the processes were only experimentally achievable in the pulsed laser regime, making precise experimental comparisons difficult. Since then, cw NDOPOs have been experimentally realized and have received a good deal of theoretical attention ([31], and references therein). But not until recently has the cw Raman process been so isolated from the complicating effects of the single-photon transitions. Indeed, the experimental realization of the far-off-resonance cw Raman laser now allows for detailed comparison with the cw NDOPO. We find it fascinating that such a precise correspondence resurfaces after a 35-year hiatus.

The predicted steady-state behaviors of the two systems are identical and have been experimentally verified. They exhibit pump clamping (power limiting) behavior above threshold [16], which was first identified theoretically for the NDOPO by Siegman [32]. Furthermore, the output modes of both systems exhibit square root dependences on the input pump power, and peak photon conversion efficiencies approaching 100% at four times threshold for single-ended cavities [33, and references therein].

All of the population for both systems effectively remain in the ground state, and both systems exhibit phase insensitive amplification when only one output mode is observed. There is phase sensitivity hidden between the two output modes for the NDOPO case and between the Stokes and 1–2 coherence for the Raman case. The phase relationship for both the Raman and NDOPO cases was noted by Giordmaine [30], with the result

$$\phi_p = \phi_s + \phi_{12} + \pi/2 \tag{35}$$

for the Raman case. Both systems also exhibit the attractive feature of frequency insensitive gain. In other words, the gain is nearly the same for visible and near-infrared pump lasers. This is afforded by the large detuning from any single-photon transitions in both the Raman and NDOPO systems and allows for large frequency tuning ranges and spectral coverages of the emitted light [34].

The only formal difference between these systems lies in what has become the fundamental difference between parametric and stimulated processes [35]; that is, the NDOPO must cope with phase matching difficulties, while the cw Raman laser must deal with heat deposition. There are also differences on a more practical level that can cause their behaviors to deviate from Eqs. (24)–(26) and from one another [23,36].

There also exist less direct connections between the cw Raman laser and the standard (based on population inversion) laser. For instance, when the atomic variables can be eliminated, one can associate the population inversion of the normal laser with the intracavity pump photon number of the NDOPO and the Raman systems. Consequently, it is the population inversion that is clamped above threshold in the normal laser rather than the intracavity pump power ([37], p. 514).

In light of the similarities between the Raman and the NDOPO systems, it is natural to think that an alternative form of the Raman Hamiltonian, similar to that of the NDOPO, may be valid. Indeed, such an alternative Hamiltonian does exist and can significantly simplify the quantum mechanical treatment of the cw Raman system. By way of direct analogy with the NDOPO, we obtain the two-photon version of the Raman system Hamiltonian

$$H_{\text{sys}} = \hbar\omega_p a_p^\dagger a_p + \hbar\omega_s a_s^\dagger a_s + \hbar\omega_{21} S_{12}^\dagger S_{12}$$

$$- \hbar(g^* a_p a_s^\dagger S_{12}^\dagger + \text{H.c.}), \tag{36}$$

where g is given by Eq. (27). To be clear, this system Hamiltonian neglects all single-photon interactions, Stark shifts, and power broadening, and assumes all the population remains in the ground state. The decay and noise processes associated with level 3 are also implicitly ignored with this system Hamiltonian. It describes only the effects of the two-photon Raman process. Note also that the S_{12} operator now exhibits the bosonlike commutation relation $[S_{12}, S_{12}^\dagger] = 1$ when the upper state population is negligible. With this and including the noise and decay contributions, one can quickly derive Eqs. (24)–(26), using the Heisenberg equation of motion. Some authors have successfully applied Hamiltonians similar to Eq. (36), but with S_{12} replaced by a phonon operator, to the Raman systems (see, for instance, Ref. [1]). The Raman system derivation up to this point establishes the limits of validity for such an approximate Hamiltonian.

VI. INTENSITY NOISE SPECTRA

We calculate the intensity noise spectra of the emitted light in this section using the linearization procedure developed by Yamamoto [38] and others [39] and the input-output formalism developed by Collet and Gardiner [40]. These techniques have proven to be valuable tools for analyzing the spectra of parametric systems [29,41,42] as well as the sys-

tems that explicitly involve atomic degrees of freedom [3,5,18].

We first adiabatically eliminate the 1–2 coherence from Eqs. (24)–(26) above because its decay rate is by far the fastest of those remaining and we are concerned only with the dynamics of the light. The two field operator equations become

$$\dot{a}_p = -\kappa_p a_p - G_1 a_s a_s^\dagger a_p + i\sqrt{2G_1} a_s S_{12}^{\text{in}} + \sqrt{2\kappa_{p,0}} a_{p,0}^{\text{in}}$$
$$+ \sqrt{2\kappa_{p,1}} a_{p,1}^{\text{in}} + \sqrt{2\kappa_{p,L}} a_{p,L}^{\text{in}}, \tag{37}$$

$$\dot{a}_s = -\kappa_s a_s + G_1 a_p a_p^\dagger a_s + i\sqrt{2G_1} a_p (S_{12}^{\text{in}})^\dagger + \sqrt{2\kappa_{s,0}} a_{s,0}^{\text{in}}$$
$$+ \sqrt{2\kappa_{s,1}} a_{s,1}^{\text{in}} + \sqrt{2\kappa_{s,L}} a_{s,L}^{\text{in}}, \tag{38}$$

where $G_1 \equiv |g|^2/\gamma_{12}$. The forms of these equations are identical to previous semiclassical results except for the addition of the input noise contributions [43].

We next perform an amplitude-phase expansion on the operators using the relation $a_q = \bar{a}_q e^{-i\phi_q}$ and similarly for all the input operators. Other authors note that such an expansion is valid when the photon number is much larger than unity [38, and references therein]. The expansion decouples the amplitude behaviors from those of the phases. This is convenient because we are only interested in the amplitude behavior for the purposes of direct detection. Alternatively, a field quadrature expansion can also be performed on Eqs. (37) and (38), which yields identical noise spectra [29].

The two amplitude operator equations that result from the amplitude-phase expansion look identical to Eqs. (37) and (38) except that the operators are all replaced by amplitude operators. We then make an explicit distinction between the semiclassical steady-state field amplitudes and the small amplitude fluctuations about these stable mean values for linearization purposes. Specifically, we define the amplitude fluctuation operator $\delta\bar{a}_q(t)$ through the relation

$$\bar{a}_q(t) = |\alpha_q| + \tfrac{1}{2}\delta\bar{a}_q(t), \tag{39}$$

where $|\alpha_q| \equiv \langle \bar{a}_q \rangle$ represents the real-valued steady-state semiclassical field amplitude for large photon number and the factor of 1/2 is included for later mathematical convenience. The input fluctuation operators are represented in a manner analogous to Eq. (39). However, only the input pump operator has a nonzero mean deterministic value. All the other input operators represent purely stochastic noise and fluctuate about zero mean values.

The operator definitions given by Eq. (39) can be inserted into the two amplitude operator equations. This generates the relations for both the semiclassical steady-state amplitudes and the amplitude fluctuations. For the steady-state semiclassical behavior above threshold, we obtain

$$|\alpha_p| = \sqrt{\frac{\kappa_s}{G_1}} \quad \text{and} \quad |\alpha_s| = \sqrt{\frac{h\kappa_p}{G_1}}, \tag{40}$$

for the intracavity field amplitudes where

$$h \equiv \sqrt{r_p} - 1, \tag{41}$$

and the pump rate and threshold are defined by

$$r_p \equiv \frac{|\alpha_p^{\text{in}}|^2}{|\alpha_p^{\text{th}}|^2} \quad \text{and} \quad |\alpha_p^{\text{th}}|^2 = \frac{\kappa_p^2 \kappa_s \tau_{rt}^2}{G_1 T_{p,0}}. \tag{42}$$

The qualitative steady-state behaviors given by Eqs. (40)–(42) are identical to those obtained by previous classical and semiclassical methods [17,43], which accurately describe experimental observations. Specifically, the intracavity pump clamps above threshold and the semiclassical intracavity Stokes power grows as the square root of the pump rate. This consistency with the previous results and experiments strengthens the validity of the present method.

We note, however, that several factors prohibit G_1 from representing a quantitatively accurate estimate of the Raman gain. First, spatial aspects such as focusing of the pump and the Stokes beams inside the cavity were not addressed. Second, many significant atom-photon interactions and the RWA were neglected in this treatment for the sake of simplicity. However, these omissions only modify the Raman gain (and therefore the laser threshold) quantitatively; they do not alter the qualitative behavior of the system. Furthermore, the omissions are rendered insignificant by the fact that, in practice, the Raman gain is obtained through empirical means. See Ref. [17] to connect G_1 to empirically based Raman gain parameters and to include spatial considerations. The steady-state behavior given by Eqs. (40) and (41), as well as the noise spectra results that we will now derive do not depend on G_1 (they are all given in terms of the pump rate) and are therefore quantitatively accurate.

By inserting Eq. (39) into the two amplitude operator equations we also generate the amplitude fluctuation equations. Here, we assume that the steady-state field amplitudes are very large compared to the associated fluctuations so that second-order fluctuation terms can be neglected. As a result, the time-dependent equations for the fluctuation operators (signified by δ's) are linear and can be written in the compact form

$$\frac{d}{dt}\delta\mathbf{a}(t) = -\underline{\mathbf{A}}\,\delta\mathbf{a}(t) + \underline{\mathbf{B}}\,\delta\mathbf{S}^{\text{in}}(t) + \underline{\mathbf{C}}\,\delta\mathbf{a}_0^{\text{in}}(t) + \underline{\mathbf{D}}\,\delta\mathbf{a}_1^{\text{in}}(t)$$
$$+ \underline{\mathbf{E}}\,\delta\mathbf{a}_L^{\text{in}}(t), \tag{43}$$

where it is understood that all the fluctuation operators are functions of time and the following vectors and matrices have been defined

$$\delta\mathbf{a} = \begin{pmatrix} \delta\bar{a}_p \\ \delta\bar{a}_s \end{pmatrix}, \quad \delta\mathbf{S}^{\text{in}} = \delta\bar{S}_{12}^{\text{in}} \begin{pmatrix} 1 \\ 1 \end{pmatrix}, \tag{44}$$

$$\delta\mathbf{a}_0^{\text{in}} = \begin{pmatrix} \delta\bar{a}_{p,0}^{\text{in}} \\ \delta\bar{a}_{s,0}^{\text{in}} \end{pmatrix}, \quad \delta\mathbf{a}_1^{\text{in}} = \begin{pmatrix} \delta\bar{a}_{p,1}^{\text{in}} \\ \delta\bar{a}_{s,1}^{\text{in}} \end{pmatrix}, \tag{45}$$

$$\delta\mathbf{a}_L^{\text{in}}=\begin{pmatrix}\delta\tilde{a}_{p,L}^{\text{in}}\\[4pt]\delta\tilde{a}_{s,L}^{\text{in}}\end{pmatrix}, \tag{46}$$

$$\underline{\mathbf{A}}=\begin{pmatrix}\kappa_p+G_1|\alpha_s|^2 & 2G_1|\alpha_p||\alpha_s|\\[4pt]-2G_1|\alpha_p||\alpha_s| & \kappa_s-G_1|\alpha_p|^2\end{pmatrix}$$
$$=\begin{pmatrix}(1+h)\kappa_p & 2\sqrt{h\kappa_p\kappa_s}\\[4pt]-2\sqrt{h\kappa_p\kappa_s} & 0\end{pmatrix}, \tag{47}$$

$$\underline{\mathbf{B}}=\begin{pmatrix}-\sqrt{2G_1}|\alpha_s| & 0\\[4pt]0 & \sqrt{2G_1}|\alpha_p|\end{pmatrix}$$
$$=\text{diag}(-\sqrt{2h\kappa_p},\sqrt{2\kappa_p}), \tag{48}$$

$$\underline{\mathbf{C}}=\text{diag}(\sqrt{2\kappa_{p,0}},\sqrt{2\kappa_{s,0}}), \tag{49}$$

$$\underline{\mathbf{D}}=\text{diag}(\sqrt{2\kappa_{p,1}},\sqrt{2\kappa_{s,1}}), \tag{50}$$

$$\underline{\mathbf{E}}=\text{diag}(\sqrt{2\kappa_{p,L}},\sqrt{2\kappa_{s,L}}). \tag{51}$$

Note that we have used the relations given by Eqs. (40) and (41).

In order to generate noise spectra, we take the Fourier transform of Eq. (43) and solve for the intracavity field fluctuations (in the frequency domain) to give

$$\delta\tilde{\mathbf{a}}(\omega)=(i\omega+\underline{\mathbf{A}})^{-1}[\underline{\mathbf{B}}\,\delta\tilde{\mathbf{S}}^{\text{in}}(\omega)+\underline{\mathbf{C}}\,\delta\tilde{\mathbf{a}}_0^{\text{in}}(\omega)$$
$$+\underline{\mathbf{D}}\,\delta\tilde{\mathbf{a}}_1^{\text{in}}(\omega)+\underline{\mathbf{E}}\,\delta\tilde{\mathbf{a}}_L^{\text{in}}(\omega)], \tag{52}$$

where the operators in the Fourier space are denoted with tilde's and are defined by

$$\delta\tilde{\mathbf{a}}(\omega)=\frac{1}{\sqrt{2\pi}}\int_{-\infty}^{\infty}dt\,\delta\mathbf{a}(t)e^{i\omega t}, \tag{53}$$

and similarly for the input operators.

To transform the set of intracavity equations given by Eq. (52) to fluctuation equations outside the back of the cavity, we use the cavity boundary conditions [40]

$$\delta\tilde{\mathbf{a}}_1^{\text{out}}(\omega)=\underline{\mathbf{D}}\,\delta\tilde{\mathbf{a}}(\omega)-\delta\tilde{\mathbf{a}}_1^{\text{in}}(\omega), \tag{54}$$

where the vector $\delta\mathbf{a}_1^{\text{out}}$ is composed of output fluctuation operators outside the back mirror (denoted by subscript 1). Inserting Eq. (52) into Eq. (54) yields

$$\delta\tilde{\mathbf{a}}_1^{\text{out}}(\omega)=\underline{\mathbf{D}}(i\omega+\underline{\mathbf{A}})^{-1}\underline{\mathbf{B}}\,\delta\tilde{\mathbf{S}}^{\text{in}}(\omega)+\underline{\mathbf{D}}(i\omega+\underline{\mathbf{A}})^{-1}\underline{\mathbf{C}}\,\delta\tilde{\mathbf{a}}_0^{\text{in}}(\omega)$$
$$+[\underline{\mathbf{D}}(i\omega+\underline{\mathbf{A}})^{-1}\underline{\mathbf{D}}-\underline{\mathbf{I}}]\delta\tilde{\mathbf{a}}_1^{\text{in}}(\omega)$$
$$+\underline{\mathbf{D}}(i\omega+\underline{\mathbf{A}})^{-1}\underline{\mathbf{E}}\,\delta\tilde{\mathbf{a}}_L^{\text{in}}(\omega), \tag{55}$$

where $\underline{\mathbf{I}}$ is the identity matrix.

The output intensity noise spectra relative to the standard quantum limit are given by the diagonal elements of the matrix $\mathbf{V}^{\text{out}}(\omega)=\langle\delta\tilde{\mathbf{a}}^{\text{out}}(\omega)[\delta\tilde{\mathbf{a}}^{\text{out}}(\omega)]^{\dagger}\rangle$. Taking the input noise to be vacuum $[\langle\delta\tilde{S}_{12}^{\text{in}}(\omega)[\delta\tilde{S}_{12}^{\text{in}}(\omega)]^{\dagger}\rangle=1$, for example] in all cases but the front pump input noise $[\langle\delta\tilde{a}_{p,0}^{\text{in}}(\omega)[\delta\tilde{a}_{p,0}^{\text{in}}(\omega)]^{\dagger}\rangle\equiv V_{p,0}^{\text{in}}(\omega)$ for this case], we obtain the following analytical expressions for the emitted relative Stokes noise:

$$V_{s,1}^{\text{out}}(\omega)=1+\frac{8\kappa_s\kappa_{s,1}\{\omega^2+2\kappa_p\kappa_{p,0}h[V_{p,0}^{\text{in}}(\omega)-1]+\kappa_p^2(1-h^2)\}}{\omega^4+[\kappa_p^2(1+h)^2-8\kappa_p\kappa_sh]\omega^2+16\kappa_p^2\kappa_s^2h^2}, \tag{56}$$

and the transmitted pump noise

$$V_{p,1}^{\text{out}}(\omega)=1+\frac{4\kappa_{p,0}\kappa_{p,1}[V_{p,0}^{\text{in}}(\omega)-1]\omega^2+32\kappa_p\kappa_{p,1}\kappa_s^2h}{\omega^4+[\kappa_p^2(1+h)^2-8\kappa_p\kappa_sh]\omega^2+16\kappa_p^2\kappa_s^2h^2} \tag{57}$$

out the back of the cavity. By performing the same steps, but solving for the spectra emitted from the front mirror, we obtain

$$V_{p,0}^{\text{out}}(\omega)=V_{p,0}^{\text{in}}(\omega)+\frac{4[V_{p,0}^{\text{in}}(\omega)-1][\kappa_{p,0}^2-\kappa_p\kappa_{p,0}(1+h)]\omega^2+32\kappa_p\kappa_{p,0}\kappa_s^2h}{\omega^4+[\kappa_p^2(1+h)^2-8\kappa_p\kappa_sh]\omega^2+16\kappa_p^2\kappa_s^2h^2}, \tag{58}$$

for the reflected pump spectra. The Stokes spectra emitted from the front mirror is identical to Eq. (56) with $\kappa_{s,1}\to\kappa_{s,0}$. The steady-state expressions given by Eqs. (40)–(42) and the noise spectra given by Eqs. (56)–(58) are the primary mathematical results derived in this work.

VII. ANALYSIS

We first compare the predictions of Eqs. (56) and (57) with the semiclassical numerical technique described in Ref. [43]. Using the parameters from that reference, Figs. 2 and 3

show the predicted noise spectra at four times threshold ($h=1$) from Eqs. (56) and (57) as solid lines. The dotted lines are the predictions from Ref. [43]. All the curves are normalized to the standard quantum limit (SQL).

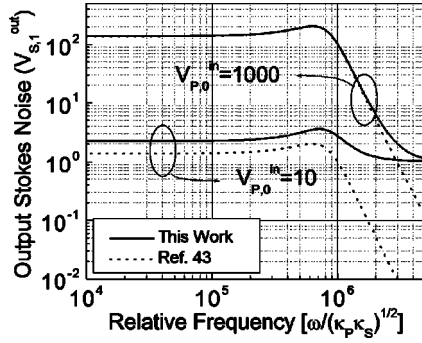Two sets of curves are provided in both figures. The upper

FIG. 2. Plot of the Stokes intensity noise relative to the SQL as a function of the Fourier frequency. The solid curves represent the predictions from Eq. (56), while the dotted curves represent those of Ref. [43]. The upper set of curves shows the noise spectra for a flat input pump noise 1000 times the SQL, while the lower set shows that for an input pump of 10 times the SQL. Discrepancies between the two theories are observed when the noise is near or below the SQL, as expected.

sets show the responses for input pump noise levels of 1000 times the SQL, while the lower sets show those for $V_{p,0}^{\text{in}}(\omega)=10$. As expected, the two theories closely agree for large noise levels, but deviate for low noise levels near or below the SQL. This is simply because the treatment given in Ref. [43] does not include quantum noise contributions, while the present treatment does. We emphasize that the noise predictions of Ref. [43], and therefore those of the present work, accurately describe experimental data for noise levels far above the SQL. Noise levels approaching the SQL have not yet been experimentally investigated.

We also point out that Eq. (56) exactly matches (in the appropriate limits) Eq. (3.18) from Ref. [29], which was obtained through a field quadrature expansion for the NDOPO. To confirm this, note the following: $h=s^2$, $\kappa_q=\gamma_q/2$, $\gamma_i \gg \gamma_s, \gamma_p$, and the annoying factors of 4 are avoided in the present treatment with the factor of one-half in Eq. (39). Reference [29] also demonstrates that it is possible (and informative) to decompose the output noise spectra into their constituent noise contributions.

Several limiting cases can yield insight into the physics embedded within Eqs. (56)–(58). In the high-frequency limit, the output spectra become
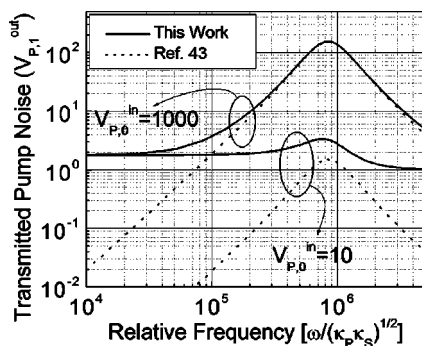

FIG. 3. Same as Fig. 2 except plotting the transmitted pump noise [Eq. (57)] instead of the output Stokes noise.

$$V_{s,1}^{\text{out}}(\omega)=V_{p,1}^{\text{out}}(\omega)=1 \quad (\omega\gg\kappa_p,\kappa_s), \quad (59)$$

$$V_{p,0}^{\text{out}}(\omega)=V_{p,0}^{\text{in}}(\omega) \quad (\omega\gg\kappa_p,\kappa_s), \quad (60)$$

for all pump rates. This indicates that the input pump fluctuations simply bounce off the input coupler when they are well above the cavity linewidths. This leaves only the reflected vacuum fluctuations for the Stokes and the transmitted pump output fluctuations in this limit.

The lower frequency limit is more interesting. For frequencies well below the cavity linewidths, Eq. (56) becomes

$$V_{s,1}^{\text{out}}(\omega)=1+\frac{1}{2h^2}\frac{\kappa_{s,1}}{\kappa_s}\left\{2h\frac{\kappa_{p,0}}{\kappa_p}[V_{p,0}^{\text{in}}(\omega)-1]+1-h^2\right\}$$

$$(\omega\ll\kappa_p,\kappa_s). \quad (61)$$

This system is very noisy near threshold ($h\ll1$), a trait that it shares with other laser systems. For very high pump rates ($h\gg1$), on the other hand, the output Stokes noise approaches $1-\kappa_{s,1}/2\kappa_s$. This indicates that noise fluctuations below the SQL are possible at high pump rates. The noise level approaches a lower limit of 50% below the SQL when $\kappa_{s,1}=\kappa_s$ (i.e., in the absence of the Stokes mirror absorption).

At a pump rate of four times the threshold value ($h=1$, $r_p=4$), the low-frequency Stokes noise simplifies to

$$V_{s,1}^{\text{out}}(\omega)=1+\frac{\kappa_{s,1}\kappa_{p,0}}{\kappa_s\kappa_p}[V_{p,0}^{\text{in}}(\omega)-1]$$

$$(\omega\ll\kappa_p,\kappa_s \text{ and } h=1). \quad (62)$$

From this result we see that for a single-ended lossless cavity ($\kappa_s=\kappa_{s,1}$ and $\kappa_p=\kappa_{p,0}$), the system displays perfect photon statistics transfer from the input pump to the output Stokes for a pump rate of four times threshold and for frequencies below the cavity linewidths, that is, $V_{s,1}^{\text{out}}(\omega)=V_{p,0}^{\text{in}}(\omega)$ for this ideal case. This is the AC analog to the 100% photon conversion efficiency that is possible in the steady-state for this particular pump rate ([33], and references therein).

Also in the low-frequency limit, Eqs. (57) and (58) become

$$V_{p,1}^{\text{out}}(\omega)=1+\frac{2}{h}\frac{\kappa_{p,1}}{\kappa_p} \quad (\omega\ll\kappa_p,\kappa_s) \quad (63)$$

and

$$V_{p,0}^{\text{out}}(\omega)=V_{p,0}^{\text{in}}(\omega)+\frac{2}{h}\frac{\kappa_{p,0}}{\kappa_p} \quad (\omega\ll\kappa_p,\kappa_s). \quad (64)$$

The transmitted pump noise given by Eq. (63) does not depend on the input pump noise. This is the AC analog to the pump clamping that is observed in the steady-state above threshold. The first term (i.e., the 1) in Eq. (63) represents the vacuum fluctuations that are reflected off of mirror 1. The
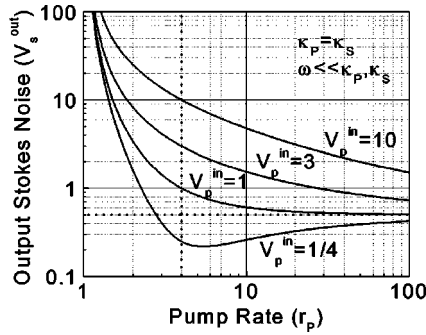
FIG. 4. Plot of the Stokes intensity noise relative to the SQL as a function of pump rate for frequencies well below the cavity linewidths. Curves for several different values of the input pump intensity noise are shown. The system exhibits perfect photon statistics transfer from pump to Stokes at four times threshold and the intensity noise approaches 50% below the SQL in the limit of large pump rate.
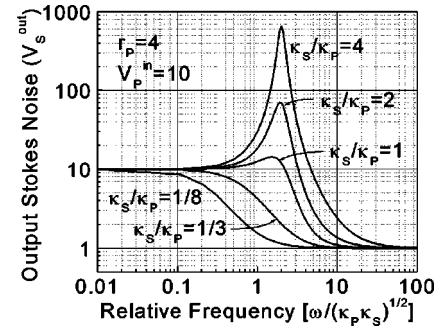

FIG. 5. The Stokes intensity noise relative to the SQL as a function of normalized Fourier frequency for several different ratios of the cavity decay rates (κ_s/κ_p) and for a pump rate of four times threshold. Decreasing the cavity decay rate of the Stokes relative to that of the pump suppresses the relaxation oscillations.

second term represents the noise transmitted through this mirror from the circulating pump. Similarly, the reflected pump noise given by Eq. (64) is composed of the reflected portion of the input pump noise (the first term) and the transmitted portion of the circulating pump noise (the second term). In both cases, larger pump rates (larger h) result in smaller contributions from the circulating pump fluctuations. The equations predict that neither of these fluctuations can dip below the SQL when the input fluctuations are classical.

For clarity, we now confine the analysis to the Stokes output from a single-ended lossless cavity ($\kappa_s = \kappa_{s,1}$ and $\kappa_p = \kappa_{p,0}$). Figure 4 illustrates the pump rate behavior of the intensity noise for the Fourier frequencies below the cavity linewidths ($\omega \ll \kappa_p, \kappa_s$) and for several different input pump noise levels. A coherent state input pump noise corresponds to $V_p^{in}(\omega) = 1$. As predicted by Eq. (61), the Stokes intensity noise is well above the SQL near threshold ($h \approx 0$, $r_p \approx 1$) for all curves, but is equal to the input pump noise $[V_s^{out}(\omega) = V_p^{in}(\omega)]$ at four times threshold ($h = 1$, $r_p = 4$) for all curves. A vertical dotted line at $r_p = 4$ is provided to emphasize this point.

Also as predicted, the output intensity noise can drop below the SQL $[V_s^{out}(\omega) = 1]$ for higher pump rates and asymptotically approaches $V_s^{out}(\omega) = 1/2$ in the limit of large pump rate ($r_p \gg 1$) even when the input pump noise is greater than the SQL. A horizontal dotted line at $V_s^{out}(\omega) = 1/2$ is provided in Fig. 4 to emphasize this point.

The behavior between the extremely low and extremely high-frequency limits depends critically on the ratio of the two cavity decay rates. Figures 5 and 6 help illustrate the issues involved. Figure 5 shows the Stokes intensity noise as a function of Fourier frequency for a pump rate of four times threshold ($h = 1$, $r_p = 4$) and an input pump noise ten times greater than the SQL $[V_p^{in}(\omega) = 10]$. Several curves are given corresponding to several different values of the cavity decay rate ratio (κ_s/κ_p). The Fourier frequency on the horizontal axis is given relative to $\sqrt{\kappa_p \kappa_s}$ to maintain a constant threshold for all curves. As the decay rate ratio increases, relaxation oscillations become undamped as evidenced by the in-

creasing noise peak in the figure. In general, decreasing the cavity decay rate ratio (i.e., making the Stokes cavity finesse greater than that of the pump) suppresses these relaxation oscillations. This is consistent with previous findings in the time domain [44].

The relaxation oscillation behavior is also dependent on the pump rate. This is illustrated in Fig 6. The figure shows the normalized intensity noise as a function of the Fourier frequency for the symmetric case when $\kappa_p = \kappa_s$ and for an input pump noise of ten times the SQL. Several curves are provided corresponding to different pump rates. The relaxation oscillations are diminished and pushed to higher frequencies as the pump rate is increased. Also note that $[V_s^{out}(\omega) = V_p^{in}(\omega)]$ for the four-times-threshold curve at low frequencies. In general, increasing the pump rate yields broadband noise suppression.

Figure 4 implies that with a sufficiently quiet pump source, and for a sufficiently high pump rate, intensity squeezing can be observed. However, this is only true for the Fourier frequencies below the cavity linewidths. Unfortunately, the desire for large cavity linewidths directly competes with the desire for large pump rates because an increase in the cavity bandwidths necessarily results in an increase in the threshold. This is a common dilemma found
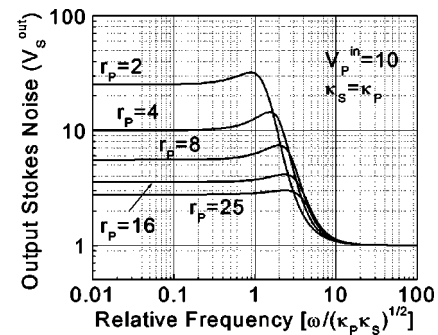

FIG. 6. The Stokes intensity noise relative to the SQL as a function of normalized Fourier frequency for several different pump rates, equal cavity decay rates ($\kappa_s = \kappa_p$) and for an input pump noise of $V_p^{in}(\omega) = 10$. Increasing the pump rate suppresses the relaxation oscillations and pushes them to higher frequencies.

in many other nonlinear optical systems and poses a significant obstacle to experimentally generating intensity noise levels below the SQL for this system.

VIII. SUMMARY

In this work, we presented the quantum theory of the far-off-resonance cw Raman laser using the Heisenberg-Langevin approach. The large single-photon detuning and moderate Rabi frequencies present in the system provided the means for significant simplification of the quantum Langevin equations. These simplifications enabled us to establish a strong connection between this cw Raman system and the cw NDOPO.

We linearized the simplified quantum Langevin equations in order to generate analytical expressions for the output noise spectra from this laser system. We showed that both the steady-state and the time-dependent results were consistent with previous semiclassical treatments in the appropriate

limits. We also showed that perfect photon statistics transfer from the pump to the Stokes can occur for low Fourier frequencies when a single-ended lossless cavity is pumped at four times threshold. For higher pump rates, we predict that this system can exhibit 50% noise reduction below the SQL within the cavity bandwidths. In order to suppress relaxation oscillations in the system, we showed that the most favorable operational conditions were high pump rate ($r_p \gg 1$) and low ratio of cavity decay rates ($\kappa_s \ll \kappa_p$). In other words, the cavity finesse for the Stokes should be greater than that of the pump and the threshold should be as low as possible.

ACKNOWLEDGMENTS

---

[1] A. Miranowicz and S. Kielich, in *Modern Nonlinear Optics*, Part 3, edited by M. Evans and S. Kielich, Advances in Chemical Physics Series Vol. LXXXV (Wiley, New York, 1994), pp. 531–626.

[2] C.M. Savage and D.F. Walls, Phys. Rev. A **33**, 3282 (1986).

[3] T.C. Ralph, C.C. Harb, and H.-A. Bachor, Phys. Rev. A **54**, 4359 (1996).

[4] A. Imamoglu, J. Field, and S. Harrisr, Phys. Rev. Lett. **66**, 1154 (1991).

[5] K.M. Gheri and D.F. Walls, Phys. Rev. A **45**, 6675 (1992).

[6] K.M. Gheri and D.F. Walls, Phys. Rev. Lett. **68**, 3428 (1992).

[7] S.E. Harris and A.V. Sokolov, Phys. Rev. Lett. **81**, 2894 (1998).

[8] N.N. Bogolubov, Jr., F.L. Kien, and A.S. Shumovsky, J. Phys. (Paris) **47**, 427 (1986).

[9] N.N. Bogolubov, Jr., F.L. Kien, and A.S. Shumovsky, Europhys. Lett. **4**, 281 (1987).

[10] C.C. Gerry and J.H. Eberly, Phys. Rev. A **42**, 6805 (1990).

[11] S. Rebic, A.S. Parkins, and D.F. Walls, Opt. Commun. **156**, 426 (1998).

[12] H. Ritsch, M.A.M. Marte, and P. Zoller, Europhys. Lett. **19**, 7 (1992).

[13] H. Ritsch and M.A.M. Marte, Phys. Rev. A **47**, 2354 (1993).

[14] K.J. Schernthanner and H. Ritsch, Phys. Rev. A **49**, 4126 (1994).

[15] A. Eschmann and R.J. Ballagh, Phys. Rev. A **60**, 559 (1999).

[16] J.K. Brasseur, K.S. Repasky, and J.L. Carlsten, Opt. Lett. **23**, 367 (1998).

[17] P. A. Roos, Ph.D. thesis, Montana State University, Department of Physics, 2002.

[18] J.Ph. Poizat, M.J. Collett, and D.F. Walls, Phys. Rev. A **45**, 5171 (1992).

[19] M.K. Olsen, K.M. Gheri, and D.F. Walls, Phys. Rev. A **50**, 5289 (1994).

[20] C.W. Gardiner and M.J. Collett, Phys. Rev. A **31**, 3761 (1985).

[21] P.A. Roos, L.S. Meng, and J.L. Carlsten, J. Opt. Soc. Am. B (to be published).

[22] P.A. Roos, J.K. Brasseur, and J.L. Carlsten, J. Opt. Soc. Am. B **17**, 758 (2000).

[23] J. Bienfang, W. Rudolph, P.A. Roos, L.S. Meng, and J.L. Carlsten, J. Opt. Soc. Am. B **19**, 1318 (2002).

[24] L.S. Meng, P.A. Roos, and J.L. Carlsten, Opt. Lett. **27**, 1226 (2002).

[25] C.W. Gardiner and P. Zoller, *Quantum Noise*, 2nd ed. (Springer-Verlag, Berlin, 1999).

[26] D.F. Walls and G.J. Milburn, *Quantum Optics*, 1st ed. (Springer-Verlag, Berlin, 1994).

[27] M.G. Raymer, J. Mostowski, and J.L. Carlsten, Phys. Rev. A **19**, 2304 (1979).

[28] M.O. Scully and M.S. Zubairy, *Quantum Optics*, 1st ed. (Cambridge University Press, New York, 1997).

[29] G. Björk and Y. Yamamoto, Phys. Rev. A **37**, 125 (1988).

[30] J.A. Giordmaine, in *Handbook of Optics*, Proceedings of the International School of Physics, edited by R.J. Glauber (Academic Press, New York, 1967), pp. 493–520.

[31] M. Ebrahimzadeh and M.H. Dunn, in *Handbook of Optics*, 2nd ed., edited by M. Bass (McGraw-Hill, New York, 2001), Vol. 4, Chap. 22, pp. 22.1–22.72.

[32] A.E. Siegman, Appl. Opt. **1**, 739 (1962).

[33] P.A. Roos, L.S. Meng, and J.L. Carlsten, J. Opt. Soc. Am. B **19**, 1310 (2002).

[34] L.S. Meng, K.S. Repasky, P.A. Roos, and J.L. Carlsten, Opt. Lett. **25**, 472 (2000).

[35] R.W. Boyd, *Nonlinear Optics*, 1st ed. (Academic Press, New York, 1992).

[36] M.J. Lawrence, R.L. Byer, M.A. Arbore, and J.D. Kmetec, Opt. Lett. **26**, 1087 (2001).

[37] A.E. Siegman, *Lasers*, 1st ed. (University Science Books, Mill Valley, CA, 1986).

[38] Y. Yamamoto, S. Machida, and O. Nilsson, Phys. Rev. A **34**, 4025 (1986).

[39] S. Reynaud, C. Fabre, E. Giacobino, and A. Heidmann, Phys. Rev. A **40**, 1440 (1989).

[40] M.J. Collett and C.W. Gardiner, Phys. Rev. A **30**, 1386 (1984).

[41] S. Reynaud and A. Heidmann, Opt. Commun. **71**, 209 (1989).

[42] C. Fabre, E. Giacobino, A. Heidmann, L. Lugiato, and S. Reynaud, Quantum Opt. **2**, 159 (1990).

[43] J.K. Brasseur, P.A. Roos, K.S. Repasky, and J.L. Carlsten, J. Opt. Soc. Am. B **16**, 1305 (1999).

[44] P.A. Roos, L.S. Meng, and J.L. Carlsten, in *Cavity-Enhanced Spectroscopies*, edited by R.D. van Zee and J.P. Looney, Experimental Methods in the Physical Sciences Vol. 40, 1st ed. (Academic Press, New York, 2002), Chap. 5.